Journal of Catalysis 413 (2022) 812–820

Contents lists available at ScienceDirect

Journal of Catalysis

journal homepage: www.elsevier.com/locate/jcat

Comparative investigation of Ga- and In-CHA in the non-oxidative ethane dehydrogenation reaction

Jian Pan [a], Jason Lee [a], Muyuan Li [a], Benjamin A. Trump [b], Raul F. Lobo [a,*]

[a] Center for Catalytic Science and Technology, Department of Chemical and Biomolecular Engineering, University of Delaware, Newark, DE 19716, United States
[b] Center for Neutron Research, National Institute of Standards and Technology, Gaithersburg, MD 20899, United States

ARTICLE INFO

Article history:
Received 2 March 2022
Revised 14 July 2022
Accepted 17 July 2022
Available online 1 August 2022

Keywords:
Alkane dehydrogenation
Activation energy
Reaction mechanism
Oxidative addition
Sustainable chemistry

ABSTRACT

Ga- and In-exchanged chabazite (CHA) zeolites with same Si/Al and metal/Al ratios were prepared via the incipient wetness impregnation method, were characterized using N_2 adsorption, electron microscopy, temperature-programed reactions and were evaluated for the ethane dehydrogenation reaction using flow microreactors. Ga-CHA has higher reaction rates and a lower activation energy of 107 kJ/mol than In-CHA (E_a = 175 kJ/mol). Rietveld refinement of the X-ray powder diffraction pattern shows that the In^+ cation is predominantly located above the 6-ring of the CHA cage. It is proposed that the reaction proceeds through the alkyl mechanism based on stability of alkyl hydride intermediates as determined using DFT calculations. The oxidative addition of ethane to the metal shows much lower Gibbs free energy for Ga-CHA (+27.95 kJ/mol) vs In-CHA (+124.85 kJ/mol). These results indicate that oxidative addition may be the rate-limiting step of ethane dehydrogenation in these materials.

1. Introduction

Catalytic non-oxidative ethane dehydrogenation is a promising approach to producing ethylene in a way that minimizes energy consumption and greenhouse gas emissions [1–4]. Although there are catalytic processes for the non-oxidative dehydrogenation of propane (such as the Oleflex process based on Pt catalysts and the Catofin process based on Cr catalysts), in practice ethane dehydrogenation is carried out thermally, not catalytically, using ethane steam crackers. The higher selectivity of catalytic non-oxidative dehydrogenation helps reduce separation costs and energy consumption, and it is easier to heat-integrate with hydrogen combustion [5–7]. More effective catalysts for non-oxidative dehydrogenation of ethane are thus urgently needed [8–10].

Metal-exchanged zeolites have been widely investigated for alkane dehydrogenation reactions [11–18]. For example, Ga impregnated in H-ZSM5 and then reduced to form Ga-ZSM5, has been reported as an effective catalyst for alkane dehydrogenation. Rane et al. investigated the propane dehydrogenation (PDH) reaction over Ga-ZSM5 and found that the activities of potential active sites are in the order of GaO^+ > Ga^+ > $[GaH_2]^+$ [11]. Schreiber et al., in contrast, claimed Lewis–Brønsted acid pairs to be the active sites and proposed a bifunctional mechanism, i.e., heterolytic activation of the propane C—H bond followed by monomolecular elimination of H_2 and desorption of propene [12]. Nascimento et al. carried out DFT studies of Ga-ZSM-5 materials and claimed that the differences in size and type of alkanes may result in distinct reaction mechanisms [13]. Running ethane dehydrogenation over Ga-ZSM5, Ausavasukhi et al. observed higher activity with the introduction of H_2. They proposed that $[GaH_2]^+$ has higher activity than either Ga^+ or GaO^+ for EDH even though $[GaH_2]^+$ is less stable than Ga^+ during EDH [14]. The structure of the active sites in Ga-ZSM5, thus, remains unclear and there are several potential candidates (Ga^+, GaO^+, and $[GaH_2]^+$ and others) that continue to be investigated. Indium, as a metal in the same group IIIA of gallium, has also been used for alkane dehydrogenation, but mostly as promoter to form In-Pt alloy supported on hydrotalcite Mg(Al)O. The introduction of In can reduce acidity strength, enhance activity, and decrease coke formation [19–22]. Reports about inclusion of mere In in zeolites, however, are very few.

At least three mechanisms have been proposed to explain the catalytic activity of these materials: i. The alkyl mechanism that starts with activation of C—H bond and the formation of M−C_2H_5, ii. The carbenium mechanism, where a zeolitic oxygen bound ethoxide along with a M−H bond is firstly formed before the formation of dihydrogen, and iii. concerted mechanism, where cleavage of two C—H bonds occur simultaneously to generate ethylene and hydrogen together [7].

Other zeotypes may also play a key role in adjusting the catalytic activity of metal species, among which the chabazite (CHA) zeolite is an example that has not been investigated in detail.

* Corresponding author.
E-mail address: lobo@udel.edu (R.F. Lobo).

https://doi.org/10.1016/j.jcat.2022.07.018
0021-9517/

The structure and smaller pore size of the CHA zeolite are likely to affect catalytic properties: species larger than propane or butane may, for example, be trapped inside the smaller cages of this zeolite leading to coke formation. Maeno et al. recently prepared In-CHA by reductive solid-state ion-exchange and studied ethane dehydrogenation properties using in situ FTIR and DFT methods [15]. This catalyst exhibits very high selectivity and durability; and an active site, $[InH_2]^+$, was proposed. To the best of our knowledge, the Ga-exchanged CHA has not been investigated in detail for this reaction and the catalytic and mechanistic differences between In- and Ga-CHA have yet to be determined.

Herein, we investigate and compare the catalytic properties for ethane dehydrogenation over In- and Ga-CHA catalysts using a combination of experimental and theoretical methods. The migration of both In and Ga species from outside to inside of the CHA micropores after reduction was monitored by N_2 adsorption isotherms and XRD powder diffraction. Analysis of ethane dehydrogenation rates yield a higher specific reaction rate and low activation energy on Ga-CHA versus In-CHA. These differences may be explained by the lower Gibbs free energy for oxidative addition of ethane to Ga(I) in Ga-CHA, as determined by DFT methods. Compared with other supports (Al_2O_3 and SiO_2), Ga-CHA has higher turnover frequency (TOF) due to the stabilization of reaction intermediates by the small pore structure and metal cation coordination environment. Higher Si/Al ratio on Ga-CHA improves turnover frequency. After calcination and reduction, the spent Ga-CHA recovers nearly all its initial catalytic activity.

2. Experimental section

2.1. Catalyst preparation

NH_4-CHA zeolite samples with Si/Al ratio of 6 were obtained from ACS Material LLC (California, USA). NH_4-CHA with Si/Al ratios of 12 and 21 were synthesized according to previously reported procedures [23,24]. Prior to testing, all samples were calcined at 550 °C for 10 h in flowing air with a ramping rate of 2 °C/min to obtain the acid form of the zeolite (H-CHA). In- and Ga-CHA with various Ga/Al and Si/Al ratios were prepared via incipient wetness impregnation (IWI) with aqueous solution of indium (III) nitrate hydrate (99.999 %, Sigma Aldrich) and gallium (III) nitrate hydrate (99.9 %, Sigma Aldrich). γ-Al_2O_3 (powder) and SiO_2 (silica gel, G-6) were obtained from Alfa Aesar and Fuji Silysia, respectively. γ -Al_2O_3 and SiO_2 supports were calcined in flowing air at 600 °C for 8 h by heating ramp rate of 2 °C/min to remove any residual water. Ga-Al_2O_3 and Ga-SiO_2 with the same mass loading amount (9 wt% Ga) as Ga-CHA (Si/Al = 6, Ga/Al = 0.4) were prepared using a previously reported method [25,26]. The resultant In- and Ga-CHA, Ga-Al_2O_3, and Ga-SiO_2 samples were dried at 80 °C for 12 h, followed by calcination at 550 °C for 10 h in flowing air with a ramping rate of 2 °C/min to form In_2O_3 or Ga_2O_3 on the supports. After loading in the reactor, the samples were reduced under a flow of 20 mL/min of 40 % H_2/He for one hour (500 °C for In-CHA, 720 °C for Ga-CHA) in the reactor before testing for the ethane dehydrogenation reaction. To identify the various samples succinctly, catalyst samples are designated as In- or Ga-CHA (Si/Al ratio, metal/Al ratio). For example, Ga-CHA with Si/Al and Ga/Al ratios of 6 and 0.4 respectively is represented as "Ga-CHA (6, 0.4)".

2.2. Catalyst characterization

The Si/Al, In/Al, and Ga/Al ratios were determined by energy-dispersive X-ray (EDX) analysis on a JEOL JSM 7400F scanning electron microscope (SEM) and X-ray fluorescence (XRF) analysis on a Rigaku Supermini 200 WDXRF. The JEOL JSM 7400F scanning electron microscope and Zeiss Auriga 60 high resolution focused ion beam & scanning electron microscope were used to obtain SEM images and determine particle size and catalyst sample morphology. Powder X-ray diffraction (XRD) patterns were collected on a Bruker D8 diffractometer using a Cu Kα radiation (40 kV, 40 mA). For powder XRD refinements, samples loaded in capillaries (Charles Supper, 15-BG) were dehydrated in a Micromeritics VacPrep 061 degasser at 473 K for 12 h. The capillaries were then sealed with vacuum grease and epoxy in a desiccant filled air bag. Diffraction data were collected in 0D mode at room temperature. XRD data were processed with the CMPR software [27] and analyzed using the Rietveld method with the GSAS/EXPGUI package [28,29]. Atomic occupancy for In was set as a free-to-fit variable in the refinement. The sum of Si and Al occupancies were set to 1. A previously reported structure of the CHA framework was used as a starting model for the refinement [30].

The micropore volumes of the zeolite samples were determined using the *t*-plot method; the N_2 adsorption isotherms were collected on a Micromeritics 3Flex system. Before N_2 adsorption, the samples were degassed at 300 °C for 24 h using N_2. Temperature programmed reduction profiles (TPR) were obtained under a 10 % H_2/Ar atmosphere while the amount of H_2 consumption was monitored using TCD (Micromeritics AutoChem II). The amounts of carbonaceous deposits formed on the spent catalysts were measured by thermogravimetric analysis (TGA) on Discovery TGA (TGA 550) in air. ^{27}Al MAS solid-state NMR spectra were collected on a Bruker AVIII 500NMR spectrometer equipped with a 44 mm HX MAS NMR probe under a MAS frequency of 10 kHz. In situ DRIFTS spectroscopy measurements were conducted on a Nicolet 6700 instrument equipped with a Harrick drifts cell. Ultraviolet/visible (UV/Vis) spectra of the samples were collected using a UV/Vis spectrometer (Jasco V-550) with a diffuse reflectance cell. Reflectance measurements converted to the Kubelka–Munk function:

$$F(R) = \frac{(1-R)^2}{2R} = \frac{K}{S} \quad (1)$$

where R is the ratio of the diffuse reflectance of the sample to that of a reference material ($BaSO_4$, Sigma Aldrich), K is the absorption coefficient, and S is the scattering coefficient.

2.3. Catalytic rates and catalyst evaluation

Catalysts were tested for ethane dehydrogenation in a fixed-bed plug-flow microreactor with a 6.35 mm ($^1/_4$ in) in diameter quartz tube. Typically, 50 mg of the sample (20–40 mesh) was placed in the reactor and the catalyst bed was kept in place by quartz wool plugs at the top and bottom. A thermocouple was placed right below it inside the quartz tube. There was no detectable catalytic activity with the empty reactor at the reaction temperatures investigated. After loading the catalyst, the sample was heated up to the desired reduction temperature (500 °C for In-CHA, 720 °C for Ga-CHA) with a ramping rate of 10 °C/min in 50 mL/min of He. Then, 20 mL/min of 40 % H_2/He was introduced to reduce the samples for a period of one hour, followed by purging with 50 mL/min He. After this step, the temperature was changed to the desired value for catalyst evaluation and 15 mL/min of 10 % C_2H_6/He was fed into the reactor to quantify ethane dehydrogenation rates. Apparent activation energies were determined in the temperature range of 585–645 °C using 50 mL/min of 10 % C_2H_6/He, and were measured under low conversion (<10 %) were far from equilibrium conversion. The initial data points of the experiment were collected by the GC and were used to minimize the influence of deactivation for the calculations of apparent activation energies. The reactor effluent was periodically sampled using an online gas chromatograph (GC) (Agilent 7890B) with a restek ShinCarbon column

(80486–810901) and a TCD for product analysis. The conversion of C_2H_6, selectivity of C_2H_4, and the carbon balance were determined using eqs. (2) to (4), respectively.

$$Conversion[\%] = \frac{F_{C_2H_6,in} - F_{C_2H_6,out}}{F_{C_2H_6,in}} \times 100 \quad (2)$$

$$Selectivity[\%] = \frac{2 \times F_{C_2H_4,out}}{2 \times F_{C_2H_4,out} + F_{CH_4,out}} \times 100 \quad (3)$$

$$Carbon\ balance[\%] = \frac{2 \times F_{C_2H_6,out} + 2 \times F_{C_2H_4,out} + F_{CH_4,out}}{2 \times F_{C_2H_6,in}} \times 100 \quad (4)$$

2.4. Density functional theory calculations

All calculations were performed using Gaussian 09, Revision D.01 at the M062x/def2svp level of theory [31]. Thermal corrections to the electronic energy were calculated at 298 K in the harmonic oscillator approximation.

A 106-atom quantum cluster for CHA was created using the crystal structure for In-CHA obtained via Rietveld refinement, vide infra. Based on crystallographically determined distances, the In atom was placed above the 6-membered ring of the sodalite cage in the publicly available CHA crystal structure from the database of the Structure Commission of the International Zeolite Association (IZA-SC) (Table S1). All framework atoms within 6.0 Å of the extra-framework In atom were included in the cluster (Fig. S1). Capping hydrogens were attached to dangling bonds at the boundary of the cluster and frozen in all optimization calculations to prevent the quantum cluster from deviating far from the crystal structure. The Ga-CHA cluster was created by replacing the In atom with a Ga atom. All structure parameters of possible clusters are listed in the Appendix of Supporting Information.

Both clusters were allowed to relax, resulting in the metal cation shifting closer to the single aluminum *T*-site—the crystal structure averages the *T*-site around the entire 6-membered ring due to the symmetry of the $R\bar{3}m$ space group, hence the centered "average" position for the In atom—in the cluster. These optimized geometries were used as starting points for further calculations with hydrocarbons. While searching for intermediates, the optimized geometry with the lowest energy was chosen from the calculation results of multiple starting geometries.

3. Results and discussion

3.1. Morphology and structure of In- and Ga-CHA

To compare the catalytic properties of In- and Ga-CHA, the same Si/Al ratio of 6 and In/Al or Ga/Al ratio of 0.7 were prepared, leading to In_2O_3 and Ga_2O_3 loadings of 22 wt% and 12 wt%, respectively. CHA with higher Si/Al ratios of 12 and 21 were also synthesized for Ga-CHA with the same Ga/Al ratio of 0.4 to investigate the influence of Si/Al ratio. These values were confirmed by EDX and XRF. The ^{27}Al MAS NMR spectra of H-CHA samples with different Si/Al ratios were also obtained (Fig. S2). The peak at 55–60 ppm is the tetrahedral framework Al and the peak at ~ 0 ppm is the octahedral Al which could contain both extra framework Al and framework Al coordinated to water in an octahedral [32,33] coordination environment. Even if it is assumed that the peak at ~ 0 ppm is only attributed to extra framework Al, the peak area ratio of in/extra framework is high (6.5, 8, 46 for H-CHA with Si/Al ratios of 6, 12 and 21, respectively) and we can neglect the potential influences of the existence of extra framework Al.

Two new peaks at ~ 30.8° and ~ 35.5° were observed in the XRD diffraction pattern (Fig. S3) of samples impregnated with indium nitrate and calcined afterwards; these are assigned to the (222) and (400) diffraction peaks of In_2O_3, respectively [15]. After reduction, these XRD peaks are not observed confirming the reduction of In_2O_3 and the migration of In into the zeolite pores. Impregnation and calcination of gallium nitrate on the CHA crystals does not lead to any evident change in the XRD pattern (Fig. S4) of all calcined Ga- samples. This may be due to the overlap of Ga_2O_3 peaks and CHA peaks in XRD, e.g., ~35.3° [34]. The small particles of In_2O_3 and Ga_2O_3 in calcined In-CHA and Ga-CHA can be observed on the surface of the zeolite crystals on the SEM micrographs of the samples (see Fig. 1). Similar Ga_2O_3 particles are also present in calcined Ga-CHA samples with higher Si/Al ratios of 12 and 21 (Fig. S5).

The micropore volume change of samples during the various synthesis steps has been determined using N_2 adsorption isotherms. The results evidence the movement of In and Ga into the zeolite pores upon reduction of the samples (Fig. S6 and Table 1). According to the loading of In_2O_3 (22 wt%) and Ga_2O_3 (12 wt%) after impregnation, the volume the oxides occupy inside the zeolite pores correspond to 0.03 and 0.02 cm^3/g, respectively. The as-received H-CHA (6) has an average pore volume of 0.32 cm^3/g, while the freshly prepared In- and Ga-CHA after calcination with the same Si/Al and metal/Al ratios have micropore volumes of 0.31 and 0.30 cm^3/g, respectively. These values indicate that both In_2O_3 and Ga_2O_3 are mostly present outside of the micropores of

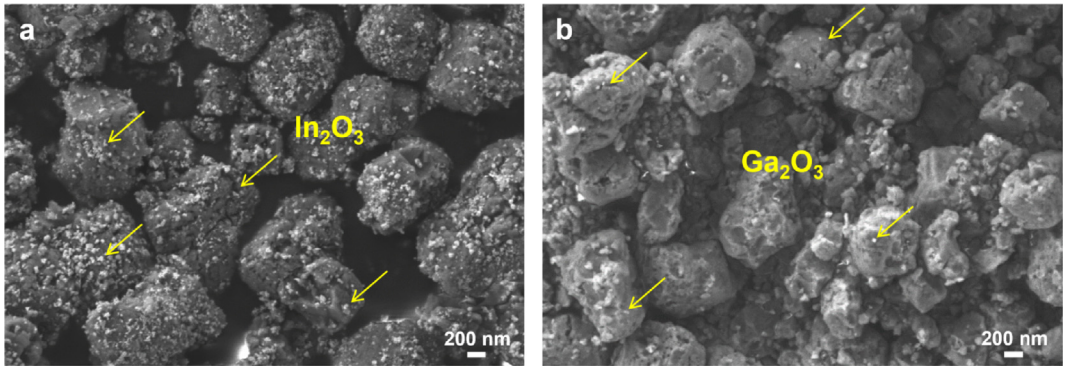

Fig. 1. SEM images of as-prepared a) In-CHA (6, 0.7) and b) Ga-CHA (6, 0.7) before reduction. In_2O_3 and Ga_2O_3 particles (~50 nm) are supported on the surface of pseudocubic H-CHA crystals.

the calcined In- and Ga-CHA samples. After reduction, however, both the pore volumes of In-CHA and Ga-CHA decrease to about 0.26 cm^3/g. The decrease of pore volume is consistent with the movement of In and Ga from outside to inside of the pores. The same trends were also observed in other Ga-CHA samples with different Ga/Al ratios (see Table 1).

Table 1
Micropore volume of In- and Ga-CHA samples before and after reduction.

Pore volume (cm^3/g)	Si/Al	In/Al or Ga/Al	Before reduction	After reduction
H-CHA	6	–	**0.32**	**–**
In-CHA	6	0.7	**0.31**	**0.26**
Ga-CHA	6	0.4	**0.30**	**0.28**
	6	0.7	**0.30**	**0.26**
	6	1	**0.30**	**0.24**
	12	0.4	**0.25**	**0.21**
	21	0.4	**0.21**	**0.19**
Ga-Al_2O_3	–	–[a]	**0.40**	**0.40**
Ga-SiO_2	–	–[a]	**0.62**	**0.62**

[a] Same Ga loading amount (9 wt% Ga) as Ga-CHA (6, 0.4).

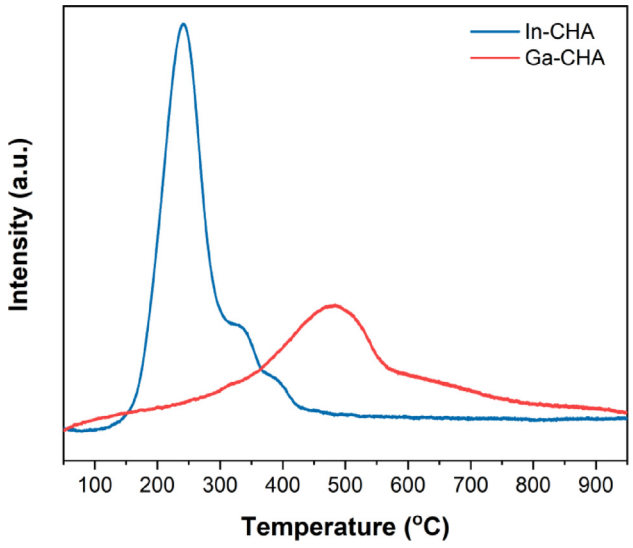

Fig. 2. H_2-TPR profiles of In- and Ga-CHA. Temperature range 50–950 °C using 10 % H_2 balance Ar.

A DRIFTS investigation using CD_3CN as the probe molecule have also been done to evaluate the acid sites change. The acetonitrile bands at ~ 2327 and 2300 cm^{-1} indicate the presence of Al_{FR} Lewis acid site (LAS) and Brønsted acid sites (BAS) [32]. Only a band at ~ 2270 cm^{-1} is observed on Ga-CHA with the Ga/Al ratio of 1, a result attributed to the interaction between CD_3CN and Ga. That is, the protons of BAS are replaced by Ga to form Ga^+ LAS. The sample of In-CHA with In/Al ratio of 0.3 show all three bands at ~ 2327, 2300, and 2270 cm^{-1}, indicating the partial replacement of BAS with In (Fig. S7).

The hydrogen temperature programmed reduction (H_2-TPR) of the impregnated In- and Ga-CHA (6, 0.7) show that higher reduction temperature is needed for Ga-CHA reduction than for In-CHA (Fig. 2). The trace for In-CHA shows three peaks at 250, 340, and 390 °C but no features are observed above 500 °C. That is, the In-CHA sample was completely reduced below 500 °C and higher reduction temperature would not influence its catalytic properties (Fig. S8). For Ga-CHA, however, the TPR profile shows maxima at 490 and 670 °C, that is, Ga-CHA is not completely reduced until about 720 °C in this experiment. Accordingly, as shown below, pre-reduction temperature does affect the catalytic properties of Ga-CHA specially at the initial stage of ethane dehydrogenation process (Fig. S9). As a result, In- and Ga-CHA samples were reduced at 500 °C and 720 °C, respectively, prior to catalytic tests.

3.2. Ethane dehydrogenation over In- and Ga-CHA

At 600 °C, Ga-CHA catalysts show higher specific reaction rates than In-CHA under same Si/Al ratio of 6 and metal/Al ratio of 0.7 (see Fig. 3a & Table 2). The initial reaction rate over Ga-CHA (21.8 mmol/g_{cat}/hr) is almost twice that of In-CHA (11.3 mmol/g_{cat}/hr). The rates of both samples decrease rapidly over the first two hours leading to rates of 12 mmol/g_{cat}/hr for Ga-CHA and 4.6 mmol/g_{cat}/hr for In-CHA after four hours on stream (Table 2). Both samples produce C_2H_4 with very high selectivity (~98 %) throughout the measurements.

Differences in selectivity and carbon balance are observed at the initial stage of the reaction for both In- and Ga-CHA. The C_2H_4 selectivity of In-CHA remains almost constant from the beginning to the end of reaction, while with Ga-CHA, the selectivity increases first from an initial value of 96.5 % to 98 % and then stabilizes. This is correlated to the accumulation of carbon-containing species in the Ga- samples (Table 1). The difference is even more clear in carbon balance (Fig. S10): Initially, both In- and Ga-CHA have their lowest observed carbon balance (90.7 % and 87.1 %, respectively),

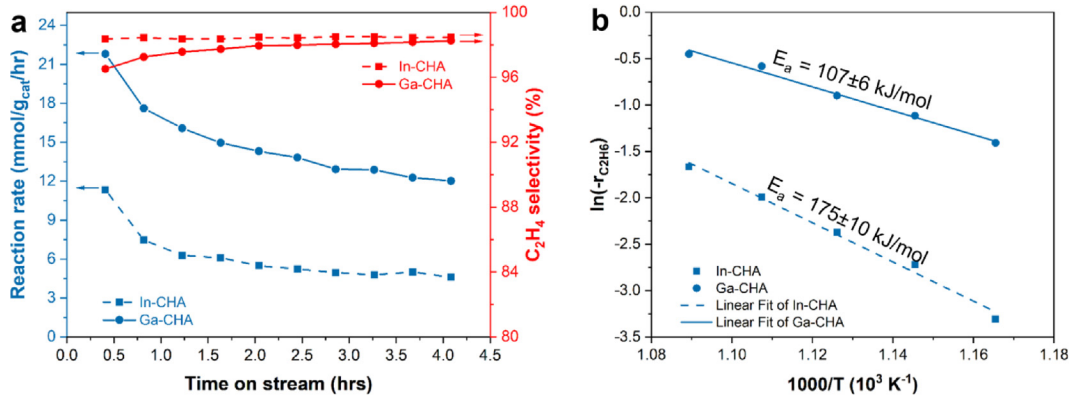

Fig. 3. Comparison between In- and Ga-CHA in a) reaction rate and C_2H_4 selectivity; b) apparent activation energy. (Reduction conditions: 20 mL/min of 40 % H_2/He at 500 °C (In-CHA) and 720 °C (Ga-CHA). Reaction conditions: a) 15 mL/min of 10 % C_2H_6/He at 600 °C; b) 50 mL/min of 10 % C_2H_6/He at 585–645 °C). Both In- and Ga-CHA have a Si/Al ratio of 6 and metal/Al ratio of 0.7.

Table 2
Reaction rates, selectivity, and carbon balance of In- and Ga-CHA at different composition and reaction time.

Sample	Time on stream (hr)	Reaction rate (mmol/g_{cat}/hr)	Selectivity (%)	Carbon balance (%)
H-CHA, Si/Al = 6	0.5	1.77	78.2	99.7
	4	0.96	76.9	100
In-CHA, (6, 0.7)[a]	0.5	11.3	98.3	90.7
	4	4.59	98.5	98.9
Ga-CHA, (6, 0.4)[a]	0.5	21.0	95.8	87.0
	4	9.82	98.3	96.9
Ga-CHA, (6, 0.7)[a]	0.5	21.8	96.5	87.1
	4	12.0	98.3	95.8
Ga-CHA, (6, 1)[a]	0.5	23.0	97.1	87.0
	4	13.6	98.2	95.8
Ga-CHA, (12, 0.4)[a]	0.5	14.9	98.4	89.4
	4	6.95	99.0	97.7
Ga-CHA, (21, 0.4)[a]	0.5	10.9	98.9	91.3
	4	3.96	99.1	99.1
Ga-Al_2O_3[b]	0.5	12.2	98.8	97.6
	4	4.42	96.2	99.3
Ga-SiO_2[b]	0.5	1.98	99.8	100
	4	2.59	99.7	100

[a] Catalyst samples are designated as In- or Ga-CHA (Si/Al ratio, metal/Al ratio).
[b] Same Ga loading amount (9 wt%) as Ga-CHA (6, 0.4).

but the carbon balance improves with time and approaches a stable value of over 95 % after four hours of time on stream (TOS), demonstrating a reduction in coke formation rate over time.

The type and amount of carbon species accumulated during the first four hours of TOS can be analyzed using UV/vis spectroscopy and thermo gravimetric analysis (TGA). The UV/vis spectra of the spent Ga-CHA catalyst have electronic transitions at 350, 400, and 450 nm (these features are not observed in the fresh Ga-CHA, see Fig. S11). These peaks can be assigned to occluded carbenium ions and aromatics moieties which are too big to move between cages and leave the CHA zeolite. These species could transform into carbonaceous solids during the reaction [35]. In contrast, no additional absorption peaks are observed on the UV/vis spectra of In-CHA after ethane dehydrogenation perhaps due to the intrinsic lower rate of In-CHA. The amount of coke formed during the catalytic test, as determined by TGA (Fig. S12), is about 0.73 % for In-CHA, and much higher (5.41 %) for Ga-CHA.

An Arrhenius plot was used to compare reaction rates at different temperatures and calculate apparent activation energies of ethane dehydrogenation using the initial data points of the experimental GC results (Fig. 3b). Between the temperatures of 585 °C and 645 °C, Ga-CHA maintains higher reaction rates than In-CHA but the difference decreases with temperature due to the higher activation energy of the In catalyst. The apparent activation energy (E_a) of EDH over In-CHA was 175 kJ/mol, while that of Ga-CHA is only 107 kJ/mol. These values are similar to the experimental activation enthalpy values reported by Maeno et al. ($\Delta H^{\ddagger}_{In\text{-}CHA}$ = 236 kJ/mol; $\Delta H^{\ddagger}_{Ga\text{-}CHA}$ = 107 kJ/mol) [9].

3.3. Ga-CHA for ethane dehydrogenation

Different Ga/Al ratios (0, 0.4, 0.7, and 1) were employed in the preparation of Ga-CHA whereby Brønsted acid sites are partially or completely replaced by Ga during reduction. Prior to reduction, the three Ga-CHA samples have a micropore volume of ~ 0.30 cm^3/g; after reduction, the Ga-CHA with Ga/Al ratio of 0.4, 0.7, and 1 have lower micropore volumes of 0.28, 0.26, and 0.24 cm^3/g, respectively (Table 1) confirming the movement of Ga into the micropores: the difference is clearly related to the different loading amount of Ga. The introduction of Ga increases both the reaction rate and C_2H_4 selectivity compared with H-CHA (Fig. 4a & Table 2). That is, the Ga-containing active sites in Ga-CHA are more reactive and selective than the Brønsted acid sites in H-CHA. Increasing the Ga/Al ratio from 0.4 to 0.7 and 1 leads to reaction rate increase due to the rise in the number of Ga sites.

Brønsted acid sites are selective for the scission of C—C bonds [36,37], generating more CH_4 from ethane and reducing selectivity towards C_2H_4 over H-CHA compared with Ga-CHA (Fig. 4b). Due to the reduction of the Brønsted acid sites number, the Ga-CHA with higher Ga/Al ratios also show higher C_2H_4 selectivity. The carbon balance of H-CHA, in contrast, is the highest due to its low reactivity (Fig. S13). The increase in coke formation with higher Ga/Al ratio is evidenced by the TGA analyses (Table S2).

With the increase of Si/Al ratio from 6 to 12 and 21, the specific reaction rate for ethane dehydrogenation decreased (Fig. S14 & Table 2) but the C_2H_4 selectivity and carbon balance increased (Fig. 5b & S13). The amount of coke determined from the TGA traces is also consistent with the carbon balance, higher carbon balance leading to less coke formation (Table S2). The apparent lower reaction rate of Ga-CHA with higher Si/Al ratio may stem from the lower loading amount of Ga in the Ga-CHA. After normalizing based on the Ga loading, Ga-CHA with higher Si/Al ratio have, in fact, higher TOF (Fig. 5a). This can be rationalized by considering the number of Ga atoms per cage as the amount of Ga increases: Since there are 36 T atoms in the CHA cage, higher Si/Al ratio decreases the number density of Al sites per cage [38] reducing interaction between sites. The presence of multiple Ga sites in a CHA cage is thus detrimental to the overall reaction rate of the samples.

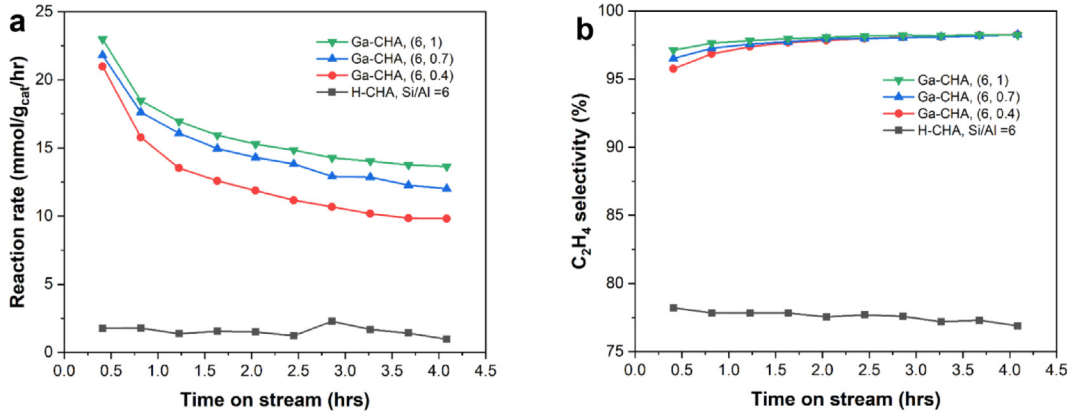

Fig. 4. Effect of Ga/Al ratio on the a) reaction rate and b) C_2H_4 selectivity of EDH over Ga-CHA with Si/Al ratio of 6 and Ga/Al ratios of 0.4, 0.7, and 1. (Reduction conditions: 20 mL/min of 40 % H_2/He at 720 °C. Reaction temperature = 600 °C, 15 mL/min of 10 % C_2H_6/He).

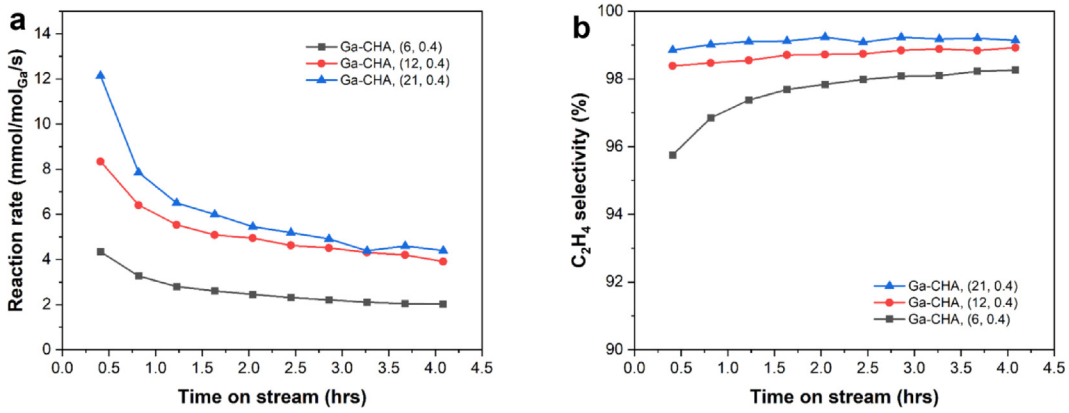

Fig. 5. Effect of Si/Al ratio on a) reaction rate (TOF or per mole of Ga) and b) C_2H_4 selectivity of EDH over Ga-CHA with Ga/Al ratio of 0.4 and Si/Al ratios of 6, 12, and 21. (Reduction conditions: 20 mL/min of 40 % H_2/He at 720 °C. Reaction temperature = 600 °C, 15 mL/min of 10 % C_2H_6/He).

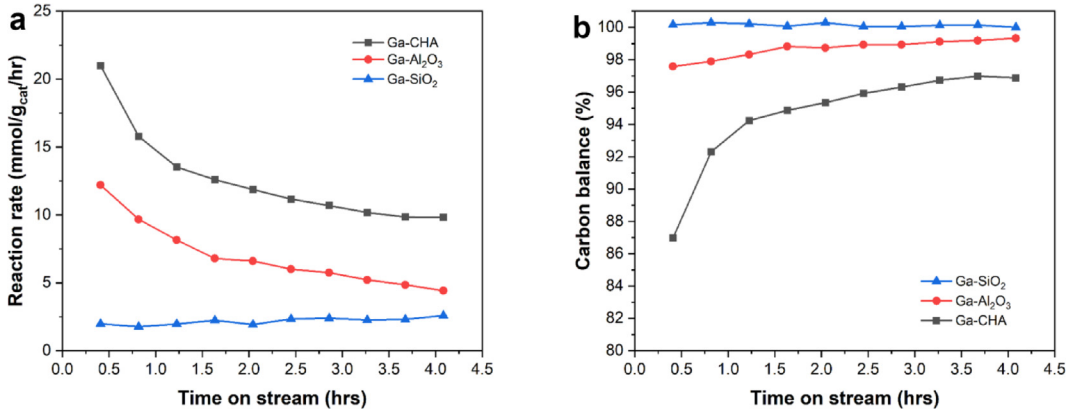

Fig. 6. Effect of the support on: a) reaction rate and b) carbon balance of EDH over Ga-CHA. Ga-Al_2O_3 and Ga-SiO_2 have the same Ga loading (9 wt% Ga) as Ga-CHA. (Reduction conditions: 20 mL/min of 40 % H_2/He at 720 °C. Reaction temperature: 600 °C, 15 mL/min of 10 % C_2H_6/He).

Compared with Al_2O_3 or SiO_2 supports, Ga-CHA has the highest specific reaction rate (Fig. 6a and Table 2). In contrast with Ga-CHA, the pore volumes of Ga-Al_2O_3 and Ga-SiO_2 do not change after reduction (Table 1). This is because no solid-state reduction and ion exchange of Ga occurs over Al_2O_3 and SiO_2 supports, that is, different active sites are being formed. The weight loss associated with coke combustion during TGA evaluations are 4.5 %, 3.9 %, and 0.46 % for Ga-CHA, Ga-Al_2O_3, and Ga-SiO_2, respectively, which is consistent with the carbon balance measured during the kinetic experiments (Fig. 6b & Table S2). However, note that the coke can be readily combusted, recovering catalytic activity of Ga-CHA manifesting the stability of active sites in Ga-CHA upon regeneration (Fig. S15).

3.4. Comparison of In- and Ga-CHA

The introduction of In and Ga species (after reduction) into the zeolite lead to high reactivity for ethane dehydrogenation with respect to H-CHA. In and Ga replace protons inside CHA zeolite cages, reducing the rate of C—C bond scission of ethane and the generation of CH_4, and leading to the much higher C_2H_4 selectivity. Ga in CHA also shows higher reactivity than In-CHA and a much lower activation energy. At the same time, oligomerization and polymerization rates of the generated C_2H_4 are higher in Ga-CHA, leading to more coke formation. This generated carbon, however, can be oxidized in air, recovering nearly all of the initial catalytic activity.

The effect of Si/Al ratio, normalized by the loading of Ga, shows that the Ga-CHA with higher Si/Al ratio has the highest TOF. This may be because, when the Si/Al ratio is higher, there are fewer Ga cations per cage or, in other words, that the Ga-Ga interactions reduce the average reaction rates [38]. Since CHA zeolite has 8-ring pores (~3.8 Å), products larger than propylene formed by Ga sites (such as aromatics), are trapped inside the zeolite cages [39].

3.5. XRD structure analysis of Ga- and In-CHA

Structural analysis of the H-CHA and In-CHA samples provides insight on coordination environments inside of the micropores of the zeolite. Diffraction data of both samples were analyzed in the trigonal space group R $\bar{3}$ m. The unit cell contains 36 symmetrically equivalent T atoms (Si or Al) and 72O atoms. In In-CHA, the In^+ cation is located above the 6-ring with an In-O distance of 2.47 Å (Fig. 7). Refinement of H-CHA diffraction pattern shows that there is no water residue left inside the pores nor metal cations within the cages (Fig. S16 and Table S3) after calcination of the ammonium exchanged sample. Refinement of In-CHA patterns shows a contraction of the unit cell volume (2346.6(4) $Å^3$) compared to that of H-CHA (2374.61(9) $Å^3$), confirming In presence in the zeolite cages and strong bonding with the framework O atoms (Fig. S17

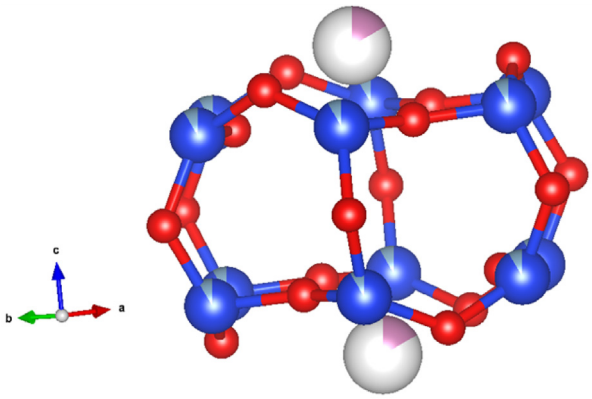

Fig. 7. Structure of the In(I) coordination site in In-CHA determined by Rietveld refinement of In-O = 2.468(7) Å. Blue spheres: Si or Al; red spheres: O; purple spheres: In. The actual In site does not possess the C3 symmetry as shown above, since the Al site is at one particular location rather than averaged distribution shown in the figure.

and Table S4). Unit cell volume of In-CHA is also smaller than the value reported by Pham et al. for K-CHA (2366.8 $Å^3$) [40], indicating In has stronger interactions with the zeolite framework compared to K.

The refined bond length of In-O is cross-compared with the M(I)-O bond length of a series of alkali metal-exchanged CHA zeolites, and the obtained value of In-O bond length is consistent with the trends in the reported M(I)-O bond lengths [40–42]. Li, Na and K exchanged CHA all have cations at the same exchange site as In (above the 6-ring). Compared to smaller Li^+-(0.78 Å) and Na^+- (0.98 Å) exchanged CHA with M(I)-O of 1.910 Å and 2.289 Å, the larger In^+ (1.32 Å) has a longer M−O distance of 2.47 Å. K^+ (1.33 Å) with similar ionic radius has a longer reported M(I)-O of 2.739 Å. The other exchange site found in K-CHA, which is at the center of 8-ring of CHA [40], is not observed in In-CHA in this study.

It should be noted that the diffraction measurement is conducted at room temperature. Under reaction temperatures the In cations could migrate to other positions in the zeolite framework or move rapidly between sites. We also found that reduced Ga-CHA is air-sensitive, and we are unable to produce diffraction patterns that could be analyzed with confidence using the Rietveld technique; thus, no results on Ga-CHA are reported.

3.6. DFT calculations of intermediates in In- and Ga-CHA for ethane dehydrogenation

Density functional theory (DFT) calculations were used to investigate potential mechanisms of ethane dehydrogenation over In- and Ga-CHA (Table S5 – 10). To determine the possible form of the active site, the energies of different oxidation states of In within the same CHA cluster model were compared. Using water and hydrogen for stoichiometric balance, In(I) was found to be the lowest energy (most stable) form when compared to $In(OH)_2$, InO, and InH_2 (Fig. S18, Table S7). This agrees with the crystal structures of In-CHA after reduction (vide supra). Although a crystal structure could not be obtained for Ga-CHA, the comparable amounts of H_2 used to reduce In_2O_3 and Ga_2O_3 in calcined In- and Ga-CHA prior to ethane dehydrogenation will likely reduce the In and Ga into stable surfaces species with at least a + 1 oxidation state. Hence, only mechanisms starting from In(I) and Ga(I) were investigated.

Three intermediates were considered for both In and Ga to compare two primary reaction mechanisms: 1) a one-step dehydrogenation involving concerted abstraction of two hydrogen atoms, and 2) a multi-step pathway involving an ethyl-hydride-metal intermediate (Z[H-M−Ethyl], oxidation state of + 3). One-step dehydrogenation produces ethylene and the hydride form of the zeolite (Z[MH_2], oxidation state of + 1) as an intermediate with a ΔE of 137.0 kJ/mol and 249.2 kJ/mol for Ga- and In-CHA, respectively. Both one-step and multi-step mechanisms lead to ethylene and the zeolite metal hydride (Fig. 8). To complete the catalytic cycle, hydrogen must associate in the reaction Z[MH_2] → Z[M] + H_2. In In-CHA, this process is downhill; in Ga-CHA uphill (ΔE = -71.6 kJ/mol and + 40.7 kJ/mol respectively).

Although additional intermediates could be considered, the multi-step pathway can be simplified into two overall reactions: 1) oxidative addition and 2) elimination (Fig. 9). The multi-step pathway parallels a mechanism proposed for ethane dehydrogenation in Ga-ZSM-5 by Pidko et al. [43] and Mansoor et al. [44] Pidko investigated two mechanisms for what is referred in Fig. 8 as "oxidative addition". The first mechanism was a one-step oxidative addition: Z[M] + Ethane → Z[H-M−Ethyl] with a $\Delta E^{\ddagger}$ of + 374 kJ/mol over Ga-ZSM-5. The second mechanism involved an ethyl-metal intermediate in the vicinity of a zeolite Brønsted acid site (Z(BAS) + [M−Ethyl]) where $\Delta E^{\ddagger}$ was + 210 kJ/mol and ΔE was + 209 kJ/mol for the reaction Z[M] + Ethane → Z(BAS) + [M−Ethyl]. The $\Delta E^{\ddagger}$ and ΔE for the reaction Z(BAS) + [M−Ethyl] → Z[H-M−E

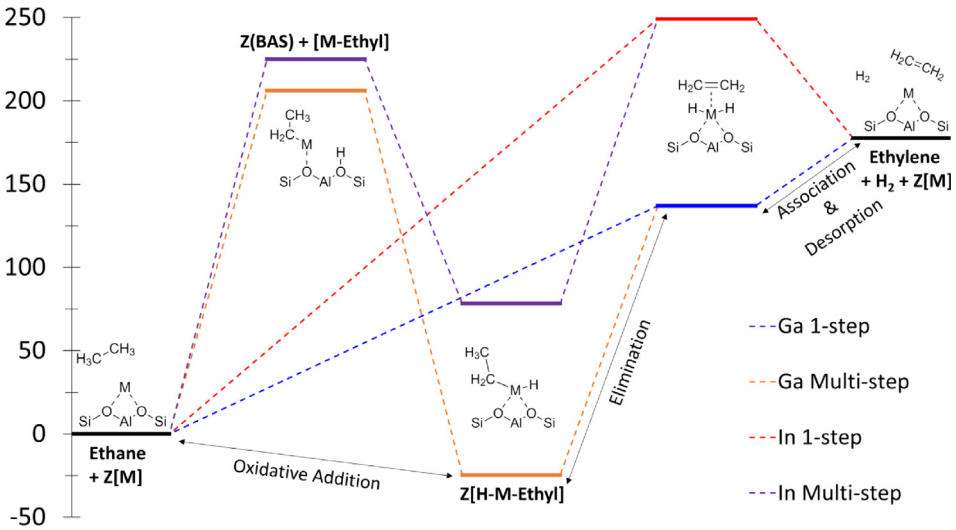

Fig. 8. Thermodynamic reaction coordinate for ethane dehydrogenation over In- and Ga-CHA.

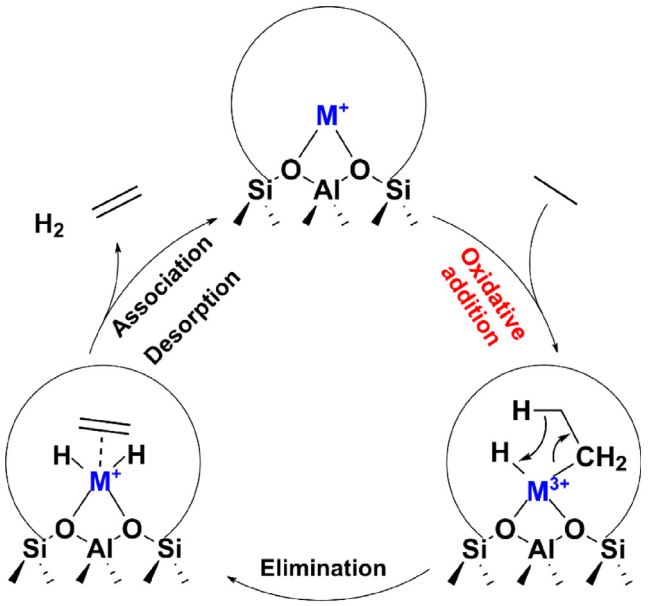

Fig. 9. Schematic diagram of ethane dehydrogenation process.

thyl] was + 9 kJ/mol and −200 kJ/mol respectively, making the first step rate determining in this mechanism.

In this work for Ga- and In-CHA, ΔE of the reaction Z[M] + Et hane → Z(BAS) + [M−Ethyl] are + 206.2 kJ/mol and + 225.0 kJ/mo l, respectively, which is remarkably similar to Pidko's value in his second "oxidative addition" mechanism (ΔE = +209 kJ/mol). Overall elimination in the reaction Z[H-M−Ethyl] → Z[MH_2] + Ethylene must begin with β-hydride elimination—the neighboring proton in the metal-proton pair will promote abstraction of the β-hydride in the ethyl group. From here, reductive elimination and ethylene desorption could generate gas-phase ethylene and hydrogen, which is what Pidko proposed for Ga-ZSM-5. Alternatively, in the one-step dehydrogenation mechanism, zeolite hydride (Z[MH_2]) and ethylene could directly generate from Z[M] + Ethane, followed by hydrogen association and ethylene desorption, as discussed earlier for Fig. 8.

From the DFT-calculated electronic energies alone, oxidative addition is far less favorable in In- than Ga-CHA (Fig. 8). Incorporating thermal corrections for free energy to calculate ΔG° at standard state (298 K, 1 atm), this trend is observed not only for ethylene, but for methane and propane as well (Table 3). For elimination, the order is reversed. Likewise, association of hydrogen is more favorable in In over Ga. Given that Ga- is more reactive than In-CHA in our experiments, the DFT results suggest that in the multi-step pathway, oxidative addition is rate controlling. The stability of the hydride based on hydrogen association/dissociation in Ga- vs In-CHA suggests that Ga's preference for a 3 + oxidation state stabilizes the reaction intermediates in comparison to the In cation. Therefore, the lower apparent activation energy of Ga-CHA is likely related to oxidative addition of ethane, which is thermodynamically more favorable than in In-CHA. This comparison provides some insights into the rate limiting elementary step. Further calculations for transition states and activation energies for all possible steps in Fig. 9 will be reported in the future.

Table 3
DFT calculated Gibbs free energy of different intermediates for alkane dehydrogenation.

Metal	Hydrocarbon	Oxidative Addition ΔG (kJ/mol)	Elimination ΔG (kJ/mol)
Ga	Methane	+16.50	+469.53
	Ethane	**+27.95**	+84.65
	Propane	−3.11	+102.81
In	Methane	+123.28	+362.71
	Ethane	**+124.85**	−12.26
	Propane	+118.26	−18.56

4. Conclusions

The catalytic properties of In- and Ga-CHA were investigated and compared using catalytic ethane dehydrogenation, powder XRD refinements and DFT calculations. Ga-CHA needs a higher reduction temperature (720 °C) than In-CHA (500 °C) for complete metal reduction and metal-ions migration into the crystal pores. Powder XRD refinements of In-CHA show that after reduction, In is located above the 6-ring of the CHA cage with an In-O distance of 2.47 Å. No clearly defined site for Ga in Ga-CHA was observed from XRD possibly due to hydration/oxidation during sample preparation.

Ga-CHA has higher reaction rates and lower activation energy (107 kJ/mol) than In-CHA (E_a = 175 kJ/mol). Higher Ga/Al ratio leads to higher specific reaction rate due to higher concentration of active Ga- species up to a Ga/Al of 1. Faster TOF is also observed with higher Si/Al ratio, which is rationalized as the effect of catalytic inhibition due to Ga-Ga interactions in a chabazite cage. Ga-CHA also shows higher dehydrogenation rate than Ga-Al_2O_3 and Ga-SiO_2 at similar loadings. Occluded aromatic species and organic cations were detected by UV/vis and TGA in the Ga-CHA samples. The small 8-ring pores of the CHA zeolite limit the movement of aromatics moieties generated from the oligomerization of C_2H_4, leading to coke accumulation and catalyst deactivation during the reaction. After calcination (and coke combustion), the catalytic properties of the Ga-CHA catalyst are regenerated.

An alkyl mechanism was proposed and investigated using DFT calculations, and the reaction intermediates formed over In- and Ga-CHA were compared. The much lower Gibbs free energy of oxidative addition over the Ga cations is consistent with the higher reactivity of Ga-CHA, which combined with the lower activation energy and higher reaction rates observed experimentally, indicates that the energetics of oxidative addition are more important than that of the elimination steps. The high selectivity and high reaction rates observed for Ga-CHA make this material a promising candidate for further development and analysis.

Data availability

Data will be made available on request.

Declaration of Competing Interest

The authors declare that they have no known competing financial interests or personal relationships that could have appeared to influence the work reported in this paper.

Acknowledgements

We acknowledge supports by the RAPID manufacturing institute, USA, supported by the Department of Energy (DOE) Advanced Manufacturing Office (AMO), award number DE-EE0007888-6.5. M.L also acknowledges the NIST Center for Neutron Research CNS Cooperative Agreement No. 70NANB17H302 for partial funding.

Note: The authors declare no competing financial interest. Certain commercial equipment, instruments, or materials are identified in this paper to foster understanding. Such identification does not imply recommendation or endorsement by the National

Institute of Standards and Technology or University of Delaware, nor does it imply that the materials or equipment identified are necessarily the best available for the purpose.

Appendix A. Supplementary data

Supplementary data to this article can be found online at https://doi.org/10.1016/j.jcat.2022.07.018.

References

[1] S. Liu, B. Zhang, G. Liu, Metal-based catalysts for the non-oxidative dehydrogenation of light alkanes to light olefins, React, Chem. Eng. 6 (1) (2021) 9–26.
[2] Y. Dai, X. Gao, Q. Wang, X. Wan, C. Zhou, Y. Yang, Recent progress in heterogeneous metal and metal oxide catalysts for direct dehydrogenation of ethane and propane, Chem. Soc. Rev. 50 (9) (2021) 5590–5630.
[3] L. Liu, A. Corma, Metal Catalysts for Heterogeneous Catalysis: From Single Atoms to Nanoclusters and Nanoparticles, Chem. Rev. 118 (2018) 4981–5079.
[4] J.C. Bricker, Advanced Catalytic Dehydrogenation Technologies for Production of Olefins, Top. Catal. 55 (19-20) (2012) 1309–1314.
[5] E.E. Stangland, Shale Gas Implications for C2–C3 Olefin Production: Incumbent and Future Technology, Annu. Rev. Chem. Biomol. Eng. 9 (1) (2018) 341–364.
[6] J.J.H.B. Sattler, J. Ruiz-Martinez, E. Santillan-Jimenez, B.M. Weckhuysen, Catalytic Dehydrogenation of Light Alkanes on Metals and Metal Oxides, Chem. Rev. 114 (20) (2014) 10613–10653.
[7] H. Saito, Y. Sekine, Catalytic conversion of ethane to valuable products through non-oxidative dehydrogenation and dehydroaromatization, RSC Adv. 10 (36) (2020) 21427–21453.
[8] Z. Yang, H. Li, H. Zhou, L. Wang, L. Wang, Q. Zhu, J. Xiao, X. Meng, J. Chen, F.-S. Xiao, Coking-Resistant Iron Catalyst in Ethane Dehydrogenation Achieved through Siliceous Zeolite Modulation, J. Am. Chem. Soc. 142 (38) (2020) 16429–16436.
[9] S. De, S. Ould-Chikh, A. Aguilar, J.-L. Hazemann, A. Zitolo, A. Ramirez, S. Telalovic, J. Gascon, Stable Cr-MFI Catalysts for the Nonoxidative Dehydrogenation of Ethane: Catalytic Performance and Nature of the Active Sites, ACS Catal. 11 (2021) 3988–3995.
[10] M. Huang, S. Yasumura, L. Li, T. Toyao, Z. Maeno, K.-I. Shimizu, High-loading Ga-exchanged MFI zeolites as selective and coke-resistant catalysts for nonoxidative ethane dehydrogenation, Catal, Sci. Technol. 12 (3) (2022) 986–995.
[11] N. Rane, A. Overweg, V. Kazansky, R. Vansanten, E. Hensen, Characterization and reactivity of Ga+ and GaO+ cations in zeolite ZSM-5, J. Catal. 239 (2) (2006) 478–485.
[12] M.W. Schreiber, C.P. Plaisance, M. Baumgärtl, K. Reuter, A. Jentys, R. Bermejo-Deval, J.A. Lercher, Lewis-Brønsted Acid Pairs in Ga/H-ZSM-5 To Catalyze Dehydrogenation of Light Alkanes, J. Am. Chem. Soc. 140 (14) (2018) 4849–4859.
[13] M.S. Pereira, A.M. da Silva, M.A.C. Nascimento, Effect of the Zeolite Cavity on the Mechanism of Dehydrogenation of Light Alkanes over Gallium-Containing Zeolites, J. Phys. Chem. C 115 (20) (2011) 10104–10113.
[14] A. Ausavasukhi, T. Sooknoi, Tunable activity of [Ga]HZSM-5 with H2 treatment: Ethane dehydrogenation, Catal. Commun. 45 (2014) 63–68.
[15] Z. Maeno, S. Yasumura, X. Wu, M. Huang, C. Liu, T. Toyao, K.-I. Shimizu, Isolated Indium Hydrides in CHA Zeolites: Speciation and Catalysis for Nonoxidative Dehydrogenation of Ethane, J. Am. Chem. Soc. 142 (2020) 4820–4832.
[16] N.M. Phadke, E. Mansoor, M. Bondil, M. Head-Gordon, A.T. Bell, Mechanism and Kinetics of Propane Dehydrogenation and Cracking over Ga/H-MFI Prepared via Vapor-Phase Exchange of H-MFI with GaCl3, J. Am. Chem. Soc. 141 (4) (2019) 1614–1627.
[17] A. Samanta, X. Bai, B. Robinson, H. Chen, J. Hu, Conversion of Light Alkane to Value-Added Chemicals over ZSM-5/Metal Promoted Catalysts, Ind. Eng. Chem. Res. 56 (39) (2017) 11006–11012.
[18] Y. Yuan, J.S. Lee, R.F. Lobo, Ga+-Chabazite Zeolite: A Highly Selective Catalyst for Nonoxidative Propane Dehydrogenation, J. Am. Chem. Soc. (2022), https://doi.org/10.1021/jacs.2c03941.
[19] P. Sun, G. Siddiqi, W.C. Vining, M. Chi, A.T. Bell, Novel Pt/Mg(In)(Al)O catalysts for ethane and propane dehydrogenation, J. Catal. 282 (1) (2011) 165–174.
[20] W. Tolek, K. Suriye, P. Praserthdam, J. Panpranot, Enhanced Stability and Propene Yield in Propane Dehydrogenation on PtIn/Mg(Al)O Catalysts with Various In Loadings, Top. Catal. 61 (15-17) (2018) 1624–1632.
[21] W. Tolek, K. Suriye, P. Praserthdam, J. Panpranot, Effect of preparation method on the Pt-In modified Mg(Al)O catalysts over dehydrogenation of propane, Catal. Today 358 (2020) 100–108.
[22] T. Srisakwattana, S. Watmanee, S. Wannakao, C. Saiyasombat, P. Praserthdam, J. Panpranot, Comparative incorporation of Sn and In in Mg(Al)O for the enhanced stability of Pt/MgAl(X)O catalysts in propane dehydrogenation, Appl. Catal. A: Gen. 615 (2021) 118053.
[23] S.I. Zones, R.A. Van Nordstrand, Novel zeolite transformations: The template-mediated conversion of Cubic P zeolite to SSZ-13, Zeolites 8 (1988) 166–174.
[24] S.I. Zones, Conversion of faujasites to high-silica chabazite SSZ-13 in the presence of N, N, N-trimethyl-1-adamantammonium iodide, J. Chem. Soc. Faraday Trans. 87 (22) (1991) 3709, https://doi.org/10.1039/ft9918703709.
[25] V.J. Cybulskis, S.U. Pradhan, J.J. Lovón-Quintana, A.S. Hock, B.o. Hu, G. Zhang, W.N. Delgass, F.H. Ribeiro, J.T. Miller, The Nature of the Isolated Gallium Active Center for Propane Dehydrogenation on Ga/SiO2, Catal. Lett. 147 (5) (2017) 1252–1262.
[26] S.P. Batchu, H.-L. Wang, W. Chen, W. Zheng, S. Caratzoulas, R.F. Lobo, D.G. Vlachos, Ethane Dehydrogenation on Single and Dual Centers of Ga-modified γ-Al2O3, ACS Catal. 11 (3) (2021) 1380–1391.
[27] B.H. Toby, CMPR - a powder diffraction toolkit, J. Appl. Crystallogr. 38 (6) (2005) 1040–1041.
[28] B.H. Toby, EXPGUI, a graphical user interface for GSAS, J. Appl. Crystallogr. 34 (2) (2001) 210–213.
[29] A.C. Larson, R.B. Dreele, B. Toby, General structure analysis system - GSAS/EXPGUI 748 (1994).
[30] Ch. Baerlocher, L.B. McCusker, Database of Zeolite Structures: http://www.iza-structure.org/databases/.
[31] M. Frisch, G. Trucks, H.B. Schlegel, G.E. Scuseria, M.A. Robb, J.R. Cheeseman, G. Scalmani, V. Barone, B. Mennucci, G. Petersson, gaussian 09, Revision d. 01, Gaussian, Inc., Wallingford CT 201 (2009).
[32] H.J. Cho, D. Kim, B. Xu, Selectivity Control in Tandem Catalytic Furfural Upgrading on Zeolite-Encapsulated Pt Nanoparticles through Site and Solvent Engineering, ACS Catal. 10 (8) (2020) 4770–4779.
[33] A. Palčić, V. Valtchev, Analysis and control of acid sites in zeolites, Appl. Catal. A: Gen. 606 (2020) 117795.
[34] L. Li, W. Wei, M. Behrens, Synthesis and characterization of α-, β-, and γ-Ga2o3 prepared from aqueous solutions by controlled precipitation, Solid State Sci. 14 (7) (2012) 971–981.
[35] Y. Jiang, J. Huang, V.R. Reddy Marthala, Y.S. Ooi, J. Weitkamp, M. Hunger, Hunger, In situ MAS NMR–UV/Vis investigation of H-SAPO-34 catalysts partially coked in the methanol-to-olefin conversion under continuous-flow conditions and of their regeneration, Microporous Mesoporous Mater. 105 (1-2) (2007) 132–139.
[36] H. Krannila, W.O. Haag, B.C. Gates, Monomolecular and bimolecular mechanisms of paraffin cracking: n-butane cracking catalyzed by HZSM-5, J. Catal. 135 (1992) 115–124.
[37] P. Shertukde, G. Marcelin, G. Sill, W. Keithhall, Study of the mechanism of the cracking of small alkane molecules on HY Zeolites, J. Catal. 136 (2) (1992) 446–462.
[38] M.J. Rice, A.K. Chakraborty, A.T. Bell, Al Next Nearest Neighbor, Ring Occupation, and Proximity Statistics in ZSM-5, J. Catal. 186 (1) (1999) 222–227.
[39] M. Moliner, A. Corma, From metal-supported oxides to well-defined metal site zeolites: the next generation of passive NOx adsorbers for low-temperature control of emissions from diesel engines, React, Chem. Eng. 4 (2019) 223–234.
[40] T.D. Pham, M.R. Hudson, C.M. Brown, R.F. Lobo, Molecular Basis for the High CO2 Adsorption Capacity of Chabazite Zeolites, ChemSusChem 7 (11) (2014) 3031–3038.
[41] B. Civalleri, A.M. Ferrari, M. Llunell, R. Orlando, M. Mérawa, P. Ugliengo, Cation Selectivity in Alkali-Exchanged Chabazite: An ab Initio Periodic Study, Chem. Mater. 15 (2003) 3996–4004.
[42] J. Emsley, S.W.R.C.D.J. Emsley, The Elements, Clarendon Press, 1998.
[43] E. Pidko, V. Kazansky, E. Hensen, R. Vansanten, A comprehensive density functional theory study of ethane dehydrogenation over reduced extra-framework gallium species in ZSM-5 zeolite, J. Catal. 240 (1) (2006) 73–84.
[44] E. Mansoor, M. Head-Gordon, A.T. Bell, Computational Modeling of the Nature and Role of Ga Species for Light Alkane Dehydrogenation Catalyzed by Ga/H-MFI, ACS Catal. 8 (7) (2018) 6146–6162.